DYNAMICS OF FINE SCALE EDDY CLUSTERS IN TURBULENT CHANNEL FLOWS

Shin-Jeong Kang, Mamoru Tanahashi and Toshio Miyauchi
Department of Mechanical and Aerospace Engineering,
Tokyo Institute of Technology
2-12-1 Ookayama, Meguro-ku, Tokyo 152-8550, Japan
E-mail: kang@navier.mes.titech.ac.jp, mtanahas@mes.titech.ac.jp, tmiyauch@mes.titech.ac.jp

ABSTRACT

To investigate dynamics of vortex clusters and large-scale structures in the outer layer of wall turbulence, direct numerical simulations of turbulent channel flows have been conducted up to $Re_\tau = 1270$. In the outer layer, the vortex clusters are composed of coherent fine scale eddies (CFSEs) of which diameter and maximum azimuthal velocity are scaled by the Kolmogorov length η and velocity u_k. The large-scale structure in the outer layer is composed of these clusters of the CFSEs, which contributes to the streamwise velocity deficit (i.e. low-momentum region). The CFSE clusters are observed in the low-momentum regions of the outer layer, and the scale of those clusters tends to be enlarged with the increase of a distance from the wall. This character is deeply related with the scale growth of the low-momentum regions (Tomkins & Adrian 2003, Tanahashi et al. 2004) in the logarithmic region. The dynamics of large-scale structures reveals that the cluster structure generated in the bottom of the logarithmic region moves downstream and its scale increases with the increase of low-momentum region. The CFSE clusters in the low-momentum regions of $u' \leq -u_{rms}$ consist of the relatively strong CFSEs, which play an important role in the production of the Reynolds shear stress and the dissipation rate of the turbulent kinetic energy. Vanishing process of the CFSE cluster is also clarified in the outer layer.

INTRODUCTION

Structure of wall turbulence has been one of the most important subjects in turbulence research because it is directly related to a lot of practical applications (e.g. drag reduction, heat transfer). In order to understand the dominant structure including streamwise vortices near the wall, many studies have been conducted for near-wall turbulence (Lyon et al. 1989, Brooke et al. 1993, Jeong et al. 1997, Heist et al. 2000, Soldati et al. 2000). The streamwise vortices are elongated in the edge of the low-speed streak and kinked above it in the near-wall region. These streamwise vortices create a shear layer by pumping low-momentum fluid from the wall (Heist et al. 2000), and the generation of those is associated with changes in the shape of the low-speed streak surface (Soldati et al. 2000). Brooke et al. (1993) have argued that the new streamwise vortex is created at the wall in the downwash of a large stress-producing eddy by using velocity vector map on a $x - z$ plane (in the present study, x, y and z axes represent streamwise, spanwise and wall-normal directions, respectively) and there is no strong interaction between the wall flow and the outer flow because the stress-producing eddies regenerate themselves. However, the streamwise vortices near the wall are stretched into the outer layer and a lot of hairpin-type vortices in the logarithmic region are connected to the streamwise vortices in the near-wall region (Adrian et al. 2000, Tanahashi et al. 2004).

The streak structures are observed not only in the near-wall region but also in the outer layer, and the lateral spacing between low-momentum regions depends on the distance from the wall and varies with Reynolds number (Tanahashi et al. 2004). The spanwise wavelengths of the maxima in pre-multiplied energy spectrum of streamwise fluctuating velocity (u') are linearly increased in the logarithmic region of turbulent boundary layer (Tomkins & Adrian 2003) and turbulent channel flows (Jiménez 1998, Kawamura et al. 2002, Álamo & Jiménez 2003). The increase of these spanwise wavelengths is caused by the low-speed streak existing in the logarithmic region, and results in the large-scale motion in wall turbulence. From particle image velocimetry (PIV) measurements on $x - y$ planes in turbulent boundary layers, Meinhart & Adrian (1995) have observed growing zones of uniform low-momentum regions in the logarithmic region. These large-scale structures are physically important because they have long lifetime and occupy large volumes in the outer layer. Adrian et al. (2000) have proposed a model based on packets of hairpin vortices from PIV measurements on $x - y$ planes in zero-pressure gradient boundary layers. They have also shown that the packets of hairpin vortices frequently occur, and coherent packets of the hairpin vortex heads appear throughout the logarithmic region. More recently, Tomkins & Adrian (2003) have suggested that the dominant large-scale motions are low u-momentum regions elongated in the streamwise direction, and the low-momentum regions are consistently associated with vortical motions at each height of y^+. However, the features of vortical motions and vortex clusters embedded in the low-momentum regions have not been investigated clearly.

From direct numerical simulation (DNS) results of turbulent flows, it has been shown that turbulence is composed of universal fine scale eddies (i.e. coherent fine scale eddies, hereafter CFSEs) which are verified in homogeneous isotropic turbulence, turbulent mixing layer and turbulent channel flows (Jiménez & Wray 1998, Tanahashi et al. 1999a, 2001, 2004). In turbulent channel flows, well-known streamwise vortices possess the same feature as the CFSEs (Tanahashi et al. 1999b), which tend to be located between the low- and high-speed streaks in the near-wall region. From the analysis of DNS data of turbulent channel flows, our previous studies (Tanahashi et al. 2004, Kang et al. 2004) have shown that the large-scale low-momentum region are composed of cluster of the CFSEs (hereafter CFSE cluster) with relatively strong rotation rate

in the outer layer. It has been inferred that these clusters also include the structure similar to the packets of hairpin vortices proposed by Adrian et al. (2000). Ganapathisubramani et al. (2003), who have performed stereoscopic PIV measurements on $x-z$ planes of turbulent boundary layers, have developed a feature identification algorithm to search for both individual hairpin vortices and packets of hairpins. From the results based on this algorithm, they have reported that hairpin packets contribute more than 25% of total Reynolds shear stress even though they occupy less than 4% of the total area.

In the present study, DNSs of turbulent channel flows up to $Re_\tau = 1270$ have been performed. From these DNS data, the CFSEs are educed to investigate a relation between the CFSE clusters and the low-momentum regions in the outer layer. The dynamics of the CFSE clusters are also discussed in connection with production of Reynolds shear stress and the energy dissipation rate.

COMPUTATIONAL APPROACH

DNSs of turbulent channel flows have been performed by solving incompressible Navier-Stokes equations and continuity equation. Spectral methods are used in the streamwise and spanwise directions, and the central finite difference method with fourth-order accuracy is used in the wall-normal direction. The aliasing errors in the streamwise and spanwise directions are completely removed by using the 3/2 rule proposed by Orszag (1971). Periodic boundary conditions are used in the streamwise (x) and spanwise (z) directions for velocity and pressure fields, and the no-slip condition is applied in the wall-normal direction (y). The computational domain sizes in x, y and z directions are selected to be $3\pi\delta \times 2\delta \times \pi\delta$ ($Re_\tau = 400$) and $2\pi\delta \times 2\delta \times \pi\delta$ ($Re_\tau = 800$ and 1270) respectively, where Re_τ is the Reynolds number based on the channel half width (δ) and the friction velocity (u_τ). Grid points are $384 \times 385 \times 192$ ($Re_\tau = 400$), $512 \times 769 \times 384$ ($Re_\tau = 800$) and $864 \times 1239 \times 648$ ($Re_\tau = 1270$), respectively.

IDENTIFICATION OF COHERENT FINE SCALE EDDIES

To investigate scaling law of the CFSEs up to $Re_\tau = 1270$ and a relation between the CFSE clusters and the low-momentum regions in the outer layer, it is necessary to identify a method for extracting vortices from instantaneous turbulent flow field. The high vorticity or enstrophy regions have been widely used to identify coherent structures and vortical structures (Hussain & Hayakawa 1987, She et al. 1990, Jiménez & Wray 1998). However, vorticity magnitude is not always appropriate method for identification of vortical structures in turbulent channel flows, since high vorticity regions represent tube-like and sheet-like structures and they exist everywhere near the wall simultaneously (i.e. for the case with a strong background shear).

Figure 1 shows the iso-surfaces of the second invariant (Q) of the velocity gradient tensor for $Re_\tau = 1270$. The second invariant of the velocity gradient tensor is given by $Q(= (W_{ij}W_{ij} - S_{ij}S_{ij})/2)$, where $S_{ij}(= (\partial u_i/\partial x_j + \partial u_j/\partial x_i)/2)$ and $W_{ij}(= (\partial u_i/\partial x_j - \partial u_j/\partial x_i)/2)$ are the symmetric and antisymmetric parts of the velocity gradient tensor $A_{ij}(= \partial u_i/\partial x_j = S_{ij} + W_{ij})$. Figure 1 indicates that turbulent channel flow consists of a lot of tube-like structures similar to homogeneous isotropic turbulence (Tanahashi et al. 1999a), turbulent mixing layer (Tanahashi et al. 2001) and

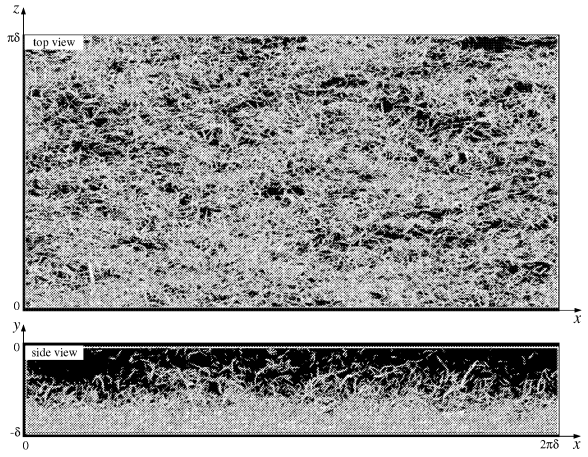

Figure 1: Contour surfaces of the positive second invariant (Q) of the velocity gradient tensor for $Re_\tau = 1270$ ($Q = 25$, domain size: $l_x \times l_y \times l_z = 2\pi\delta \times \delta \times \pi\delta$).

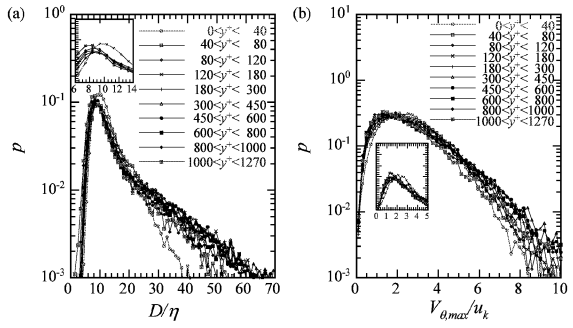

Figure 2: Probability density functions of diameter (a) and maximum azimuthal velocity (b) of the CFSEs for $Re_\tau = 1270$.

turbulent channel flows with low Reynolds number (Tanahashi et al. 2004). The density of the tube-like structures for high Reynolds number case is higher than that of lower Reynolds number cases in the unit cube of δ^3. Streamwise vortices in the near-wall region and hairpin-type vortices can be visualized with the positive Q region. However, this visualization method depends on the threshold value of the variables. Therefore, Tanahashi et al. (1999a, 2001, 2004) have developed a new identification method which can educe fine scale eddies in turbulent flows without any threshold. This identification method is based on a local flow pattern, and the educed section includes a local maximum of Q. Furthermore, three-dimensional structure of the CFSE (or axis of the CFSE) is also identified by using an axis tracing method (Tanahashi et al. 1999c, 2004) based on distributions of the positive Q region and the local flow pattern. More details about the identification method and the axis tracing method can be obtained in Tanahashi et al. (1999c, 2004).

Figure 2 shows the probability density functions (pdfs) of the diameter (D) and maximum azimuthal velocity ($V_{\theta,max}$) of the CFSEs for $Re_\tau = 1270$. These pdfs are calculated in several regions at different y^+. The diameter of the CFSE is defined as the distance between the locations where the mean azimuthal velocity shows the maximum or minimum value. The diameter and maximum azimuthal velocity are normalized by η and u_k. η and u_k are calculated from the mean

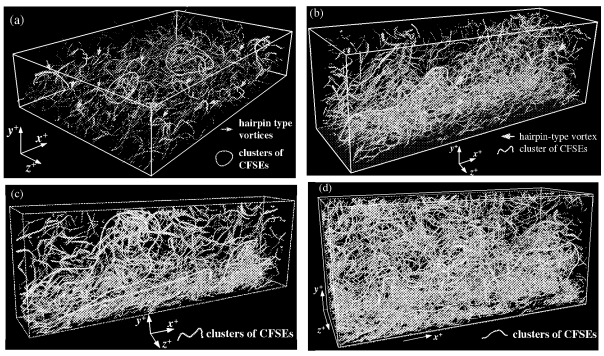

Figure 3: Spatial distributions of the axes of the CFSEs for $Re_\tau = 400$, 800 and 1270. The diameters of the axes are drawn to be proportional to $\sqrt{Q^*}$. (a): $Re_\tau = 400$, domain size: $l_x^+ \times l_y^+ \times l_z^+ = 1884 \times 400 \times 1256$ wall units, (b) and (c): $Re_\tau = 800$, domain size: $l_x^+ \times l_y^+ \times l_z^+ = 2513 \times 800 \times 780$ (b) and $l_x^+ \times l_y^+ \times l_z^+ = 2513 \times 800 \times 400$ (c), (d): $Re_\tau = 1270$, domain size: $l_x^+ \times l_y^+ \times l_z^+ = 2800 \times 1270 \times 1000$.

dissipation rate ($\overline{\epsilon}(y^+)$) of the turbulent kinetic energy at y^+. Tanahashi et al. (2004) have verified that the CFSEs can be scaled by η and u_k in turbulent channel flows up to $Re_\tau = 800$. In the near-wall region ($y^+ < 40$), the most expected D and $V_{\theta,max}$ are about 10η and $2.0u_k$, whereas they become about $8 \sim 9\eta$ and $1.2 \sim 1.8u_k$ away from the wall. In the wake region near the center of the channel, the most expected D and $V_{\theta,max}$ are about 8η and $1.2u_k$, which are very close to the values in other turbulent flows (Tanahashi et al. 1999a, 2001). These results indicate that the CFSEs in turbulent channel flows can be scaled by η and u_k up to $Re_\tau = 1270$.

CFSE CLUSTERS AND LOW-MOMENTUM REGIONS

Figure 3 shows spatial distributions of the axes of the CFSEs for all Reynolds numbers. Figure 3 (b) and (c) represent two different regions with different spanwise width for $Re_\tau = 800$. Their diameters are drawn to be proportional to the square root of Q^* on the axes, where Q^* is normalized by η and u_k at y^+ (i.e. $Q^* = Q/(u_k/\eta)^2$). Since the CFSEs in turbulent channel flows are scaled by η and u_k, the vortical structures can be visualized very well even in the regions far from the wall. These spatial distributions provide an evidence of the existence of hairpin-type vortices and groups of the CFSEs in the outer layer. In the cases of $Re_\tau = 800$ and 1270, the CFSE clusters are clearly observed because the logarithmic region is wider than that of $Re_\tau = 400$. The number density of the CFSE clusters between the near-wall region and $y/\delta = 0.5$ is higher than that of the CFSE cluster in $y/\delta > 0.5$, and the CFSE cluster in the bottom of the logarithmic region is elongated in the downstream direction. The largest cluster has a spanwise spacing of about $1100 \sim 1200$ wall units for $Re_\tau = 800$ (Tanahashi et al. 2004).

From the PIV measurements on $x - z$ planes in turbulent boundary layer, Tomkins et al. (2003) and Ganapathisubramani et al. (2003) have shown that the low u-momentum regions, which are enveloped by positive and negative vortex cores and involving the packets of the hairpin vortex, are the dominant large-scale motions in the logarithmic region. Figure 4 shows spatial distributions of the axes of the CFSEs with iso-surfaces of u'^+ for $Re_\tau = 400$, 800 and 1270. The threshold values of the iso-surfaces in Fig. 4 (a), (c) and (e)

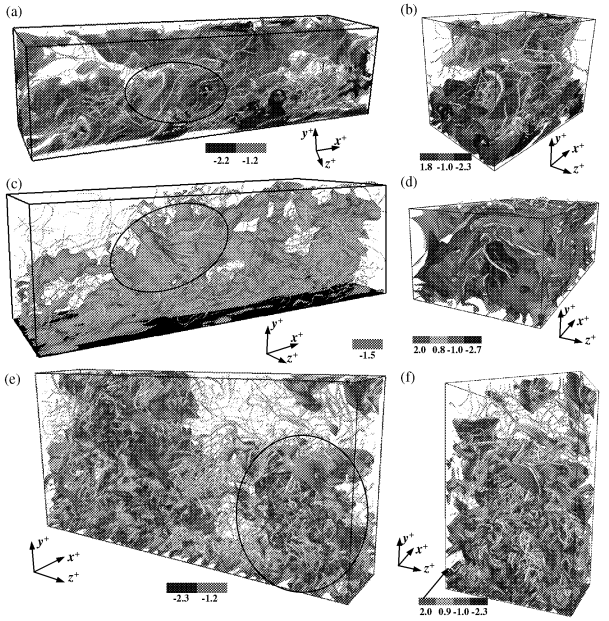

Figure 4: Spatial distributions of the axes of the CFSEs with iso-surfaces of u'^+ for $Re_\tau = 400$ (a, b), 800 (c, d) and 1270 (c, d). The diameters of the axes are drawn by the same method as in Fig. 3. Visualized domain: $l_x^+ \times l_y^+ \times l_z^+ = 1500 \times 400 \times 350$ (a), $x^+ = 400 \sim 900$, $y^+ = 0 \sim 400$ and $z^+ = 0 \sim 350$ (b), $l_x^+ \times l_y^+ \times l_z^+ = 2513 \times 800 \times 713$ (c), $x^+ = 628 \sim 2513$, $y^+ = 295 \sim 800$ and $z^+ = 0 \sim 713$ (d), $l_x^+ \times l_y^+ \times l_z^+ = 450 \times 1270 \times 2600$ (e), $x^+ = 0 \sim 450$, $y^+ = 0 \sim 1270$ and $z^+ = 1800 \sim 2600$ (f).

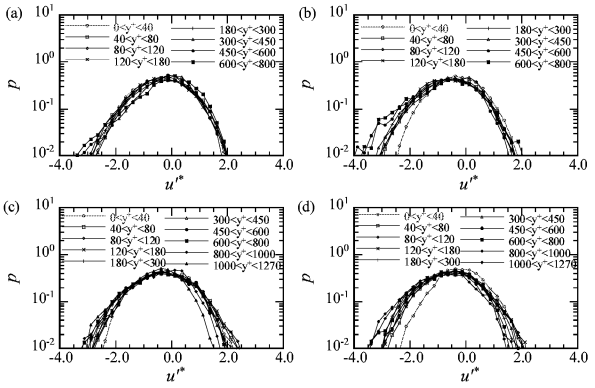

Figure 5: Conditional probability density functions of u_c^* on the axes of the CFSEs. (a) and (b): $Re_\tau = 800$, (c) and (d): $Re_\tau = 1270$. (a) and (c): $Q_c^* < \overline{Q_c^*}(y^+)$, (b) and (d): $Q_c^* \geq \overline{Q_c^*}(y^+)$.

are selected to be equal to $-u_{rms}^+$ at $y \approx 0.5\delta$. The low-momentum regions in the outer layer are composed of the CFSE clusters, which is independent of Re_τ. The regions marked by circles in Fig. 4 (a), (c) and (e) are enlarged in Fig. 4 (b), (d) and (f) in order to show a relation between the high-/low-momentum regions and the CFSE clusters in the outer layer in detail. From these visualizations, one can clearly observe that the CFSE clusters are embedded in the low-momentum regions which are surrounded by the high-momentum regions. In wall turbulence, a lot of previous studies have reported that the typical lengthscales of these low-momentum regions in the logarithmic region vary from

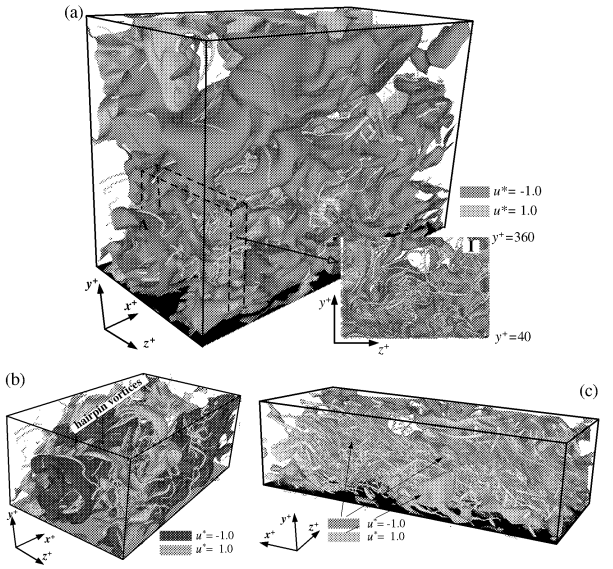

Figure 6: Low- and high-momentum regions with the CFSE axes. Visualized domains are $x^+ = 0 \sim 1200$, $y^+ = 40 \sim 860$ and $z^+ = 200 \sim 780$ (a), $x^+ = 0 \sim 940$, $y^+ = 40 \sim 400$ and $z^+ = 200 \sim 780$ (b) and $x^+ = 1200 \sim 2513$, $y^+ = 40 \sim 400$ and $z^+ = 0 \sim 500$ (c), respectively.

about δ to 3δ in the streamwise direction (Townsend 1976, Falco 1977, Jiménez 1998, Tomkins & Adrian 2003, Álamo & Jiménez 2003). These lengthscales are similar to those of the cluster structures observed in the present study.

To investigate a relation between the streak structures and the CFSEs in the outer layer quantitatively, conditional probability density functions of u_c^* $(=u'^+_c(x^+, y^+, z^+)/u^+_{rms}(y^+))$ are plotted for $Re_\tau = 800$ and 1270 in Fig. 5. Here, $u'^+_c(x^+, y^+, z^+)$ is the streamwise fluctuating velocity at the centers of the CFSEs. The pdfs are conditioned by the values of Q_c^* which is less than or greater than $\overline{Q_c^*}(y^+)$. Pdfs for $Q_c^* < \overline{Q_c^*}(y^+)$ show peaks around zero, whereas the peaks of pdfs for $Q_c^* \geq \overline{Q_c^*}(y^+)$ shift to the low-speed region (about $u_c^* \approx -0.5$). Large portion of the CFSEs exists in the low-momentum regions ($u^* \leq -1.0$) in the outer layer. This tendency is clearly observed for $Q_c^* \geq \overline{Q_c^*}(y^+)$, which is also independent of the Reynolds number. These results suggest that the low-momentum regions of $u' \leq -u_{rms}$ in the outer layer consist of many CFSEs or CFSE clusters with relatively strong swirling motions. Since the CFSEs near the wall have the same features as the streamwise vortices and are generally located in the edge of the low- and high-momentum regions, the above result can not be extended to the near-wall region.

To investigate relationship between the CFSEs and the low-momentum region at each height, iso-surfaces of streamwise fluctuating velocity normalized by the r. m. s. value at each height $(u^* = u^{'}(x^+, y^+, z^+)/u_{rms}(y^+))$ are shown in Fig. 6 with axis distributions of the CFSEs for $Re_\tau = 800$. Here the thresholds of u^* are selected to 1.0 and -1.0, respectively. Three interesting regions including the CFSE cluster in Fig. 3 (b) are visualized in Fig. 6. The low-momentum regions below about $-u_{rms}$ exist throughout the outer layer, and the inside of these low-momentum regions is composed of the CFSE cluster (see the I region in Fig. 6 (a)). A large-scale low-momentum region in the wake region ($y^+ > 300 \sim 400$ for $Re_\tau = 800$) consists of a group of the CFSEs which are

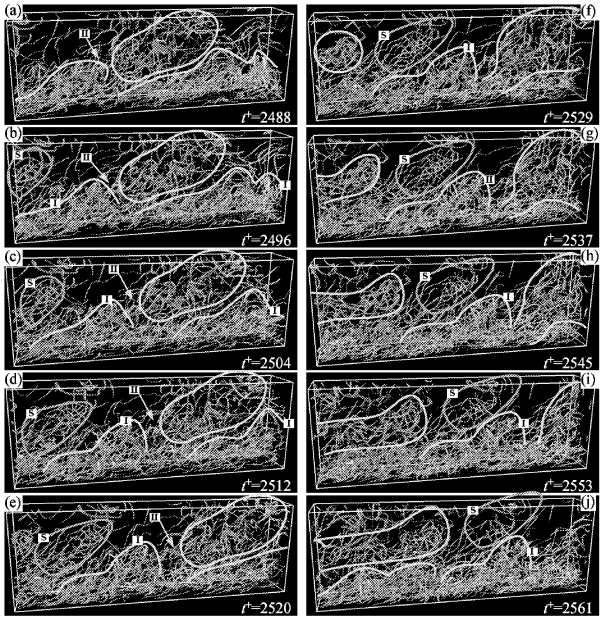

Figure 7: Temporal development of spatial distribution of the CFSEs. Visualized domain is $l_x^+ \times l_y^+ \times l_z^+ = 2356 \times 800 \times 392$.

elevated from the logarithmic region. However, the number density of the CFSEs composing the clusters in the wake region is much lower than that in the logarithmic region. This will be discussed in the next section in more detail. On the other hands, there is no CFSE cluster in the high-momentum region ($u'^* \geq 1.0$) in the outer layer. The cluster structures shown in Fig. 6 (b) and Fig. 4 (b) are very similar to the conceptual scenario (packets of hairpin vortices) proposed by Adrian et al. (2000). It should be noted that the cluster of the CFSEs dose not always possess hairpin packets type structure. Another possible structure in the logarithmic region is a bundle of the streamwise CFSEs. Figure 6 (c) shows that a uniform low-momentum region is composed of a bundle of the streamwise CFSEs with a steep inclination and hairpin-type CFSEs in the logarithmic region. The inclination angles of these streamwise vortices are $40 \sim 60$ deg or $-120 \sim -140$ deg.

DYNAMICS OF THE CFSE CLUSTER STRUCTURE

To investigate the dynamics of the large-scale structures (i.e. the CFSE clusters and low-momentum regions), the axes of the CFSEs have been extracted from time-series DNS data for $Re_\tau = 800$. Time interval and domain size of time-series DNS data are $\Delta t^+ = 8.10$ and $l_x^+ \times l_y^+ \times l_z^+ = 2512 \times 800 \times 785$ respectively, where t^+ is tu_τ^2/ν. Figure 7 shows time-series spatial distributions of the axes of the CFSEs. Note that these figures do not include the axes with a weak rotation rate at the center of the CFSEs (i.e. $Q_c^* \leq 0.8\overline{Q_c^*}(y^+)$). The scale growth and dynamics of the clusters are of particular interest in Fig. 7. There are several CFSE clusters in the outer layer in Fig. 7, and these clusters move into the downstream direction with maintaining their original features. Especially, this tendency is clearly observed in the logarithmic region. The CFSE cluster created in the bottom of the logarithmic regions tends to be elongated in the streamwise direction and stands up with small angles (about $10 \sim 20$ deg) in vertical plane (see I-zone). On the other hands, the CFSE cluster observed

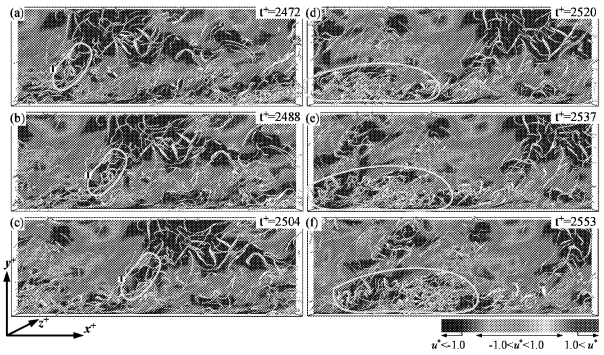

Figure 8: Distributions of $u^*(= u'(x^+, y^+, z^+)/u^+_{rms}(y^+))$ on a $x-y$ plane ($z^+ = 261$) with the CFSEs. Visualized domain is $l^+_x \times l^+_y \times l^+_z = 2356 \times 800 \times 412$.

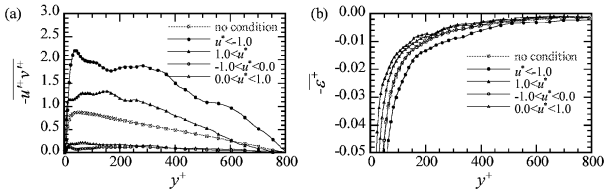

Figure 9: Mean Reynolds shear stress (a) and mean dissipation rate of the turbulent kinetic energy (b) conditioned by u^* ($Re_\tau = 800$).

in the top of the logarithmic region develops its size continuously by engulfing the CFSEs which are originally separated from the cluster in the logarithmic region (see II-zone). These results imply that the origin of the larger CFSE cluster is the CFSE cluster formed near the wall. These CFSE clusters are observed everywhere in the outer layer independent of time. The S-zone in Fig. 7 indicates a dispersing cluster (i.e. the oldest cluster) which tends to be located in regions of $|u^*| < 1.0$. Number density of the CFSEs in this cluster decreases with moving downstream, and this cluster finally extinguishes (see Fig. 7 (j)).

From the analysis of the cluster's dynamics conditioned by $u^* \geq 1.0$ and $u^* \leq -1.0$, it is verified that the CFSE clusters continuously appear in the low-momentum regions of the outer layer. As an example, Fig. 8 shows time sequence of the axes of the CFSEs with distributions of u^* on a $x-y$ plane at $z^+ = 261$. The CFSE clusters in the low-momentum regions have relatively long lifetime. These clusters move into the downstream direction with convection velocity less than $\overline{u^+}(y^+) - u^+_{rms}(y^+)$, and they are deeply related to the scale growth of the low-momentum region in the outer layer. Large-scale structure observed in the top of the logarithmic region is connected with a narrow low-momentum region and the CFSEs separated from the cluster in the logarithmic region (see I zone). From Figs. 7 and 8, a scenario of the generation of the CFSE cluster is suggested. The CFSE cluster is firstly generated in the bottom of the logarithmic region by streamwise vortices and hairpin-type vortices, and it forms a low-momentum region. As time develops, the cluster structure stands up with an angle about $10 \sim 30$ deg in vertical plane up to the wake region and its scale increases with the increase of the low-momentum region. After the cluster grows up to the largest size, eventually it extinguishes by dispersion or dissipation of the CFSEs.

Figure 9 shows the mean Reynolds shear stress ($-\overline{u'^+ v'^+}$)

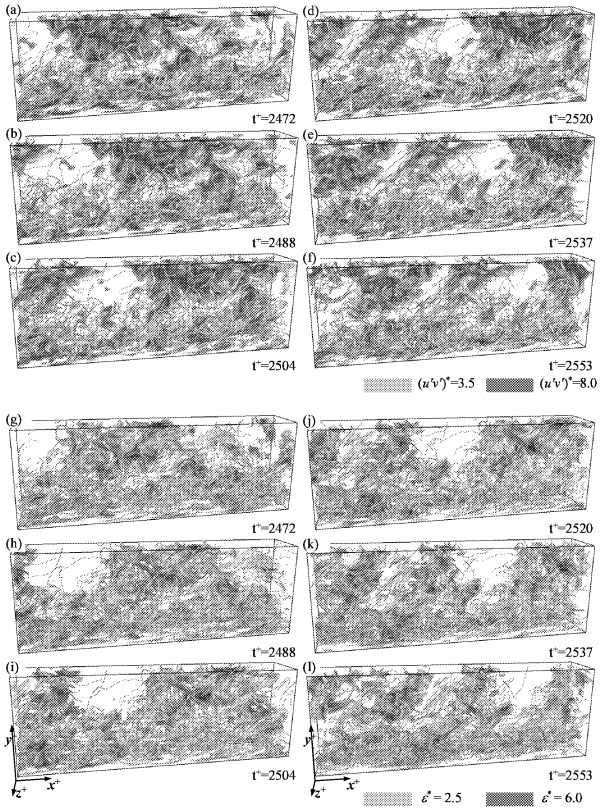

Figure 10: Instantaneous Reynolds shear stress and energy dissipation rate with the CFSEs. (a) $\sim$ (f): $(u'v')^*$ and (g) $\sim$ (l) ϵ^*. Visualized domain is $l^+_x \times l^+_y \times l^+_z = 2356 \times 800 \times 412$.

and the dissipation rate of the turbulent kinetic energy ($\overline{\epsilon^+} = 2\nu\overline{S'_{ij} S'_{ij}}$) conditioned by u^*. The mean values without the condition are also plotted for comparison. In the outer layer, the mean Reynolds shear stress in low-momentum regions ($u^* < -1.0$), which corresponds to ejection events ($u'^+ < 0.0$ and $v'^+ > 0$), shows very large values and the turbulent kinetic energy is dissipated extensively. The high-momentum regions of $u^* > 1.0$, which corresponds to sweep events ($u'^+ > 0$ and $v'^+ < 0$), also produce a significant amount of the Reynolds shear stress, whereas the energy dissipation rate in those regions shows the small value.

Figure 10 shows time sequence of the instantaneous Reynolds shear stress $(u'v')^*$ and the dissipation rate of the turbulent kinetic energy ϵ^* with the CFSE clusters. Here $(u'v')^*$ and ϵ^* denote $-u'v'(x^+, y^+, z^+)/ -\overline{u'v'}(y^+)$ and $\epsilon(x^+, y^+, z^+)/\overline{\epsilon}(y^+)$, respectively. Threshold values of the iso-surfaces are $(u'v')^*$=3.5, 8.0 and ϵ^*=2.5, 6.0. Figure 10 shows that the CFSE clusters carry a large instantaneous Reynolds shear stress ($(u'v')^* \geq 3.5 \sim 8.0$) and the turbulent kinetic energy is continuously dissipated in cluster structures. This suggests that the CFSE clusters continuously contribute to the production of Reynolds shear stress and play an important role in the dissipation mechanism of the turbulent kinetic energy. From the PIV measurements on $x-z$ planes of turbulent boundary layer, Ganapathisubramani et al. (2003) have also suggested that the packets of hairpin vortices carry a large percentage of the Reynolds shear stress. Note that the hairpin vortices are different from the CFSEs and are a sort of the CFSEs.

CONCLUSIONS

In the present study, direct numerical simulations of turbulent channel flows have been performed to investigate the clusters of vortices and their dynamics in the outer layer. The clusters of vortices are defined as aggregate of the CFSEs which are educed by our previous identification scheme (Tanahashi et al. 1999a, 2004). The diameter and maximum azimuthal velocity of the CFSEs can be scaled by η and u_k up to $Re_\tau = 1270$. In the near-wall region ($y^+ < 40$), the most expected diameter and maximum azimuthal velocity are about 10η and $2.0u_k$, whereas they become about 8η and $1.2u_k$ in the wake region near the channel center. The most expected values of those show weak y^+-dependence and have a tendency to decrease monotonically with the increase of a distance from the wall in the logarithmic region.

There are many clusters of the CFSEs in the outer layer of turbulent channel flows. The CFSE clusters form low-momentum regions in the outer layer, and these cluster structures stand up with an angle about $10 \sim 30\,\mathrm{deg}$ in vertical plane. In the outer layer, the probability of the CFSEs existing in the low-momentum regions ($u_c^* \leq -1.0$) is higher than that of the CFSEs existing in the high-momentum regions ($u_c^* \geq 1.0$), which is emphasized for the relatively strong CFSEs (i.e. $Q_c^* \geq \overline{Q_c^*}(y^+)$). These clusters are generated in the bottom of the logarithmic region, and the scale growth of those with a distance from the wall is deeply related to the scale growth of the low-momentum regions. The origin of the larger CFSE cluster in the wake region is the CFSE cluster formed near the wall, and develop its size continuously by engulfing the CFSEs originally separated from the cluster in the logarithmic region.

The mean Reynolds shear stress in the low-momentum regions ($u^* \leq -1.0$) of the outer layer shows very large values and the turbulent kinetic energy is dissipated extensively. The high-momentum regions ($u^* \geq 1.0$) in the outer layer also produce a large percentage of the Reynolds shear stress, whereas the energy dissipation rate in those regions shows the small value. A large instantaneous Reynolds shear stress ($\geq -3.5 \sim -8.0\overline{u'v'}$) is carried by the CFSE clusters and a large turbulent kinetic energy is dissipated in the cluster structures. This result suggests that the CFSE cluster structures play a very important role in the production of the Reynolds shear stress and the dissipation mechanism of the turbulent kinetic energy in turbulent channel flows.

REFERENCES

R. J. Adrian, C. D. Meinhart and C. D. Tomkins, "Vortex organization in the outer region of the turbulent boundary layer," J. Fluid Mech. 422, 1–54 (2000).

J. C. Álamo and J. Jiménez, "Spectra of very large anisotropic scales in turbulent channels," Phys. Fluids 15, L41–L44 (2003).

J. W. Brooke and T. J. Hanratty, "Origin of turbulence-producing eddies in a channel flow," Phys. Fluids A 5 (4), 1011–1022 (1993).

R. E. Falco, "Coherent motions in the outer region of turbulent boundary layers," Phys. Fluids 20, S124–132 (1977).

B. Ganapathisubramani, E. K. Longmire and I. Marusic, "Characteristics of vortex packets in turbulent boundary layers," J. Fluid Mech. 478, 35–46 (2003).

D. K. Heist, T. J. Hanratty and Y. Na, "Observations of the formation of streamwise vortices by rotation of arch vortices," Phys. Fluids 12, 2965–2975 (2000).

A. K. M. F. Hussain and M. Hayakawa, "Eduction of large-scale organized structure in a turbulent plane wake," J. Fluid Mech. 180, 193–229 (1987).

J. Jeong, F. Hussain, W. Schoppa and J. Kim, "Coherent structures near the wall in a turbulent channel flow," J. Fluid Mech. 332, 185–214 (1997).

J. Jiménez, "The largest scales of turbulent wall flows," Center for Turbulence Research Annual Research Briefs, Stanford University/NASA Ames Research, 137–154 (1998).

J. Jiménez, and A. A. Wray, "On the characteristics of vortex filaments in isotropic turbulence," J. Fluid Mech. 373, 255-285 (1998).

S.-J. Kang, M. Tanahashi and T. Miyauchi, "Coherent fine scale eddies and large-scale structures in wall turbulence," Advances in Turbulence X, 603–606 (2004).

H. Kawamura, H. Abe, Y. Matsuo and H. Choi, "Large-scale structures of velocity and scalar fields in turbulent channel flows," Proc. of Dynamics and Statistics of Coherent Structures in Turbulence: Roles of Elementary Vortices, 49–64 (2002).

S. L. Lyons, T. J. Hanratty and J. B. McLaughlin, "Turbulence-producing eddies in the viscous wall region," AIChE J. 35, 1962–1974 (1989).

C. D. Meinhart and R. J. Adrian, "On the existence of uniform momentum zones in a turbulence boundary layer," Phys. Fluids 7, 694–696 (1995).

S. A. Orszag, "Numerical simulation of incompressible flows with simple boundaries," Stud. Appl. Math. 50, 293-327 (1971).

S. K. Robinson, "Coherent motions in the turbulent boundary layer," Annu. Rev. Fluid Mech. 23, 601–639 (1991).

Z. S. She, E. Jackson and S. A. Orszag, "Intermittent vortex structures in homogeneous isotropic turbulence," Nature 344, 226–228 (1990).

A. Soldati, "Modulation of turbulent boundary layer by EHD flows," ERCOFTAC Bulletin 44, 50–56 (2000).

M. Tanahashi, T. Miyauchi and J. Ikeda, "Identification of coherent fine scale structure in turbulence," Simulation and Identification of Organized Structures in Flow, 131–140 (1999a).

M. Tanahashi, S. Shiokawa, S. K. Das and T. Miyauchi, "Scaling of fine scale eddies in near-wall turbulence," J. Jpn. Soc. Fluid Mech. 18, 256–261 (1999b).

M. Tanahashi, S. Iwase, Md. A. Uddin and T. Miyauchi, "Three-dimensional features of coherent fine scale eddies in turbulence," Proc. 1st Int. Symp. Turbulence and Shear Flow Phenomena, Begell House Inc., 79–84 (1999c).

M. Tanahashi, S. Iwase and T. Miyauchi, "Appearance and alignment with strain rate of coherent fine scale eddies in turbulent mixing layer," J. of Turbulence 2, No.6 (2001).

M. Tanahashi, S.-J. Kang, T. Miyamoto, S. Shiokawa and T. Miyauchi, "Scaling law of fine scale eddies in turbulent channel flows up to $Re_\tau = 800$," Int. J. Heat and Fluid Flow 25, 331–340 (2004).

C. D. Tomkins and R. J. Adrian, "Spanwise structure and scale growth in turbulent boundary layers," J. Fluid Mech. 490, 37–74 (2003).

A. A. Townsend, "The structure of turbulent shear flow," 2nd ed. Cambridge University Press (1976).